Optical Engineering

OpticalEngineering.SPIEDigitalLibrary.org

Stray light characteristics of the diffractive telescope system

Dun Liu
Lihua Wang
Wei Yang
Shibin Wu
Bin Fan
Fan Wu

SPIE.

Dun Liu, Lihua Wang, Wei Yang, Shibin Wu, Bin Fan, Fan Wu, "Stray light characteristics of the diffractive telescope system," *Opt. Eng.* **57**(2), 025105 (2018), doi: 10.1117/1.OE.57.2.025105.

Stray light characteristics of the diffractive telescope system

Dun Liu,[a,b,*] Lihua Wang,[a] Wei Yang,[a] Shibin Wu,[a] Bin Fan,[a] and Fan Wu[a]
[a]Chinese Academy of Sciences, Institute of Optics and Electronics, Chengdu, China
[b]University of Chinese Academy of Sciences, Beijing, China

Abstract. Diffractive telescope technology is an innovation solution in construction of large light-weight space telescope. However, the nondesign orders of diffractive optical elements (DOEs) may affect the imaging performance as stray light. To study the stray light characteristics of a diffractive telescope, a prototype was developed and its stray light analysis model was established. The stray light characteristics including ghost, point source transmittance, and veiling glare index (VGI) were analyzed. During the star imaging test of the prototype, the ghost images appeared around the star image as the exposure time of the charge-coupled device improving, consistent with the simulation results. The test result of VGI was 67.11%, slightly higher than the calculated value 57.88%. The study shows that the same order diffraction of the diffractive primary lens and correcting DOE is the main factor that causes ghost images. The stray light sources outside the field of view can illuminate the image plane through nondesign orders diffraction of the primary lens and contributes to more than 90% of the stray light flux on the image plane. In summary, it is expected that these works will provide some guidance for optimizing the imaging performance of diffractive telescopes. [DOI: 10.1117/1.OE.57.2.025105]

Keywords: diffractive telescope; diffractive optical element; ghost; stray light.

Paper 171989 received Dec. 13, 2017; accepted for publication Feb. 7, 2018; published online Feb. 26, 2018.

1 Introduction

As aperture increases, the mass of space telescope increases dramatically and the large mirror with high accuracy surface figure is difficult to fabricate. In order to solve these problems, many institutions have begun to study diffractive telescope technology.[1,2] At present, diffractive telescopes are designed based on similar principles.[3] A flat thin glass or membrane with diffractive pattern is used as primary lens to focus incident light. For removing the chromatic aberration of the diffractive lens, a relay system with complementary diffractive optical elements (DOE) must be included according to the Schupmann achromatic model. It is known that the DOEs have multiorder diffraction, but only the +1 order is used in the diffractive telescopes and the other orders may propagate to the image plane as stray light. Many publications have reported the stray light effects of DOEs in different optical system. Xiaotong Li et al. studied the ghost images caused by DOEs in the high-power laser system.[4] Their method is based on the paraxial analysis. Several works studied the effects of the diffraction efficiency on the modulation transfer function in hybrid optical system with weakly powered diffractive lens.[5–7] For diffractive telescope systems, the prototypes in "Fresnel diffractive array imager[8,9] and "membrane optic imager real-time exploitation" only verified the imaging capability of the diffractive structures.[10] But, the stray light performance of these prototypes was not considered. Recently, the diffraction efficiency and fabrication errors of the DOEs used in diffractive telescopes were studied,[11,12] but the relationship between diffraction efficiency and the imaging performance was not studied.

*Address all correspondence to: Dun Liu, E-mail: 1102444622@qq.com

In this paper, we thoroughly analyzed and tested the stray light effects in a diffractive telescope. First, a diffractive telescope prototype was developed based on the Schupmann achromatic model. Then, the optical properties and bidirectional scatter distribution function (BSDF) were given to each surface and the stray light analysis model was established. A comprehensive analysis of stray light characteristics was carried out. Nonsequential ray tracing technology and wave optical simulation were used to analyze the ghost images and the point source transmittance (PST). The veiling glare index (VGI) was calculated by integrating the PST over the full hemisphere. Finally, the test of ghost images and the VGI were carried out.

2 Stray Light Model of Diffractive Telescope

2.1 *Optical Model of Diffractive Telescope Prototype*

Based on the Schupmann achromatic model, a diffractive telescope is designed and fabricated. Figure 1(a) shows the optical schematic. There are six optical elements, two DOEs, three doublets, and one filter. The parameters of the optical elements are listed in Table 1.

DOE1 is a two-level phase Fresnel diffractive lens for collecting light. Its focal length is 800 mm when the wavelength is 550 nm and the width of the outmost zone is 11 μm. In ZEMAX, the phase function is used to describe the diffractive lens. For DOE1, the coefficients of the phase function are $a1 = -7.14$, $a2 = 2.789 \times 10^{-6}$, $a3 = -2.179 \times 10^{-12}$, $a4 = 2.278 \times 10^{-18}$, $a5 = -4.365 \times 10^{-23}$. DOE2 is also a diffractive lens for correcting the chromatic aberration of primary lens, the coefficients of the phase function are: $a1 = -58.476$, $a2 = 2.393 \times 10^{-3}$, $a3 = -3.404 \times 10^{-6}$, $a4 = -4.340 \times 10^{-9}$, $a5 = -1.443 \times 10^{-12}$.

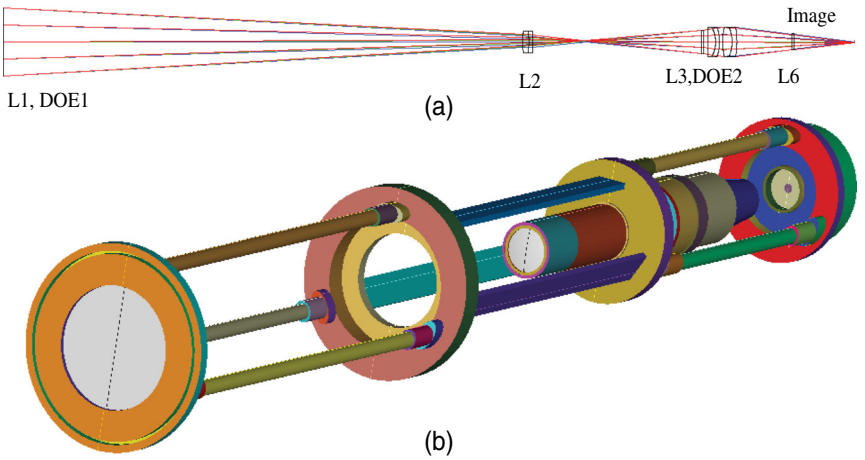

Fig. 1 (a) The optical schematic and (b) the geometry model of the prototype system.

Table 1 Main parameters of the optical elements.

	Radius of curvature	Length to next surface (mm)	Semidiameter (mm)
Front of DOE1	Infinity	0.3	40
Back of DOE1	Binary 2	661.8	40
Sur1 of L2	76.77	8	13
Sur2 of L2	−96.83	5	13
Sur3 of L2	−1267.10	215.2	13
Front of DOE2	Infinity	3	13.6
Back of DOE2	Binary 2	5	13.6
Sur1 of L4	283.1	10	17
Sur2 of L4	−33.27	5	17
Sur3 of L4	−50.35	4	17
Sur1 of L5	76.77	12	17.5
Sur2 of L5	−40.4	6	17.5
Sur3 of L5	−109.65	70	17.5
Sur1 of L6	Infinity	3	9.7
Sur2 of L6	Infinity	77.73	9.7

L2, L4, and L5 are doublets and L6 is a bandpass filter. The geometry model of the prototype is shown in Fig. 1(b), the outside shade is hidden for the sake of displaying the internal structure.

The prototype is designed to verity the imaging capabilities of diffractive telescope technology and explore possible solutions for the next large-aperture light-weight space telescope. It is also an experiment platform for studying the imaging performance of diffractive telescopes. The main parameters of the prototype are shown in Table 2 and the MTF is shown in Fig. 2. This paper focused on the stray light characteristics and intended to provide prior knowledge and experience for optimizing the imaging performance of larger aperture diffractive telescopes.

Table 2 Main parameters of the prototype.

Aperture of DOE1	Focal length	Field of view	Spectral range	Center wavelength
80 mm	361.5 mm	±0.2 deg	486 to 656 nm	550 nm

2.2 *Stray Light Source*

Stray light is the light that reaches image plane following an unintended path. These paths include specular reflection and refraction, diffraction, and random scattering.

The reflection and refraction of the optical surface subject to the Snel's law and the reflectivity and transmittance can be calculated by Fresnel formula if uncoated. Smooth surface of the mechanical structure also has specular reflection, and the reflectivity depends on the processing technology.

For binary DOEs, the diffraction efficiency η_m is given as[13]

$$\eta_m^L = \left\{\frac{\sin[\pi(m-\phi)]}{\sin(\pi(m-\phi)/L)} \times \frac{\sin(\pi m/L)}{\pi m}\right\}^2,$$
$$\phi = \frac{\lambda_0}{\lambda_i} \times \frac{\sqrt{n_i^2 - \sin^2\theta} - \cos\theta}{n_0 - 1}, \quad (1)$$

where L is the number of levels, m is the diffraction order, n_0 is the refractive index of the substrate for the design wavelength of λ_0, n_i is the refractive index for the incident wavelength λ_i, and θ is the incident angle. After passing through the DOE, the change of direction is determined as

$$l' = l + \frac{m\lambda}{2\pi} \times \frac{\partial\phi(r)}{\partial x}, \quad p' = p + \frac{m\lambda}{2\pi} \times \frac{\partial\phi(r)}{\partial y}, \quad (2)$$

where l and p are the direction cosine in x and y directions. The nondesign order diffraction of DOEs can be the dominant stray light mechanism in diffractive telescope.

Random scatter is often described by BSDF which is defined as the surface scattering radiance normalized by the incident irradiance of the surface

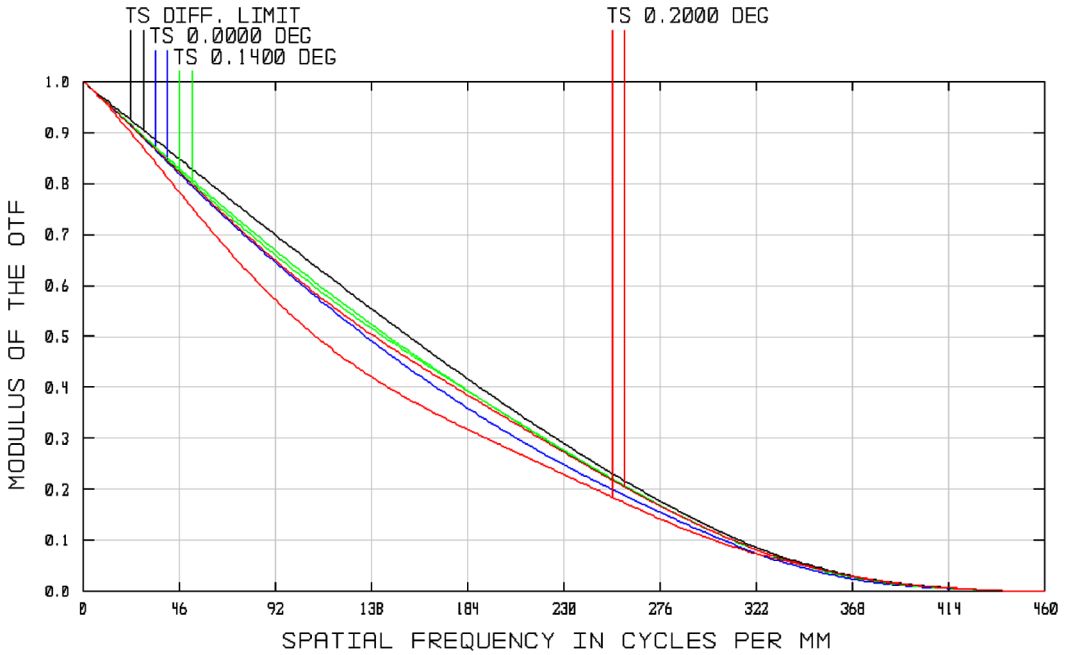

Fig. 2 The MTF of the prototype.

$$\mathrm{BSDF}(\theta_i,\phi_i;\theta_s,\phi_s)=\frac{dL(\theta_i,\phi_i;\theta_s,\phi_s)}{dE(\theta_i,\phi_i)}. \tag{3}$$

For the optically smooth surface, a Harvey BSDF model can simulate the scatter due to RMS surface microroughness σ. The functional form of Harvey BSDF[14] is

$$\mathrm{BSDF}=b_0\left[1+\left(\frac{\beta-\beta_0}{L}\right)^2\right]^{s/2}, \tag{4}$$

where $\beta=\sin(\theta_{\mathrm{scatter}})$ and $\beta_0=\sin(\theta_{\mathrm{specular}})$, b_0 is the peak value of the distribution, L is the width of the peak, and s describes the slope at large scatter angles under logarithmic coordinates. The typical value of L is 0.01 and s ranges from -2.5 to -1. Integration of Eq. (4) over the full hemisphere is the total integrated scatter (TIS) of the surface. While the TIS of optical surface has been derived independently of the BSDF as[15]

$$\mathrm{TIS}=K\cdot\left(\frac{2\pi\Delta n\sigma}{\lambda}\right)^2, \tag{5}$$

where k is the surface transmittance or reflectance, Δn is the refractive index change. Let Eq. (5) equals the integration of Eq. (4), b_0 can be calculated.

The scattering from the sharp transition regions between different zones of DOE is another source to cause stray light. A perfect Lambert scatter model is a reasonable assumption to estimate the scatter distributions and the TIS is the ratio of the transition regions to the total area.[16]

Particle contaminations may cause random scatter and the numbers of particles on a surface can be specified by the MIL-STD-1246D.[17] Based on rigorous Mie theory, the scatter characteristics can be addressed as Harvey BSDF model.[18]

2.3 *Stray Light Analysis Methods*

2.3.1 *Ghost image analysis*

Ghost images are often generated by the residual specular reflection of refractive optical elements. The path and the distribution on the image plane of ghost can be obtained directly using the nonsequential ray tracing. But tracing the collimated rays that cover the entrance aperture is a huge amount of computation and very time consuming. To solve the problem, a one-dimensional collimated ray grid is traced first. Then, the critical ghost paths can be selected according to the following conditions:

1. The number of rays in the path is greater than half the number of the imaging rays;
2. The flux of rays in the path is more than 0.01% of the imaging flux.

After that the intensity distribution of ghost images in each critical path can be analyzed one by one. For each analysis, only the reflection or diffraction of the ghost-surface that produces the ghost image in the path needs to be considered.

2.3.2 *PST calculation*

PST is frequently used to evaluate an optical system's ability to suppress stray light from outside field of view. It equals to the average detector irradiance E_{det} divided by the incident irradiance E_{inc}

$$\mathrm{PST}(\theta)=\frac{E_{\mathrm{det}}(\theta)}{E_{\mathrm{inc}}(\theta)}=\frac{P_{\mathrm{det}}(\theta)/A_{\mathrm{det}}}{P_{\mathrm{inc}}(\theta)/A_{\mathrm{inc}}}. \tag{6}$$

Before calculating PST, it is necessary to set the reasonable scattering models to each surface. Then tracing a collimated grid rays with different incident angles. The $E_{\mathrm{dec}(\theta)}$ is

the stray light flux reaching the image plane divided by the area of detector, and the PST(θ) is the ratio of $E_{\mathrm{dec}(\theta)}$ to $E_{\mathrm{inc}(\theta)}$. For the nonrotationally symmetric systems, the PST is the function of zenith angle and azimuth angle between the stray light source and the optical axis.

2.3.3 *VGI calculation*

PST describes the stray light performance of an optical system as the function of incident angle between point source and the optical axis. It cannot give an intuitive elevation of stray light background on the image plane. VGI can be used to quantify the stray light performance, and it is equal to

$$\mathrm{VGI} = \frac{E_s}{E_0 + E_s}, \tag{7}$$

where E_s is the irradiance on the center of image plane due to stray light and the E_0 is the irradiance of image. E_s can be calculated from PST by integrating it over the extended source's solid angle

$$E_0 = \frac{\pi B_0 \tau}{4F^2}. \tag{8}$$

For the optical system with small field of view, E_s can be calculated as

$$E_s = 2\pi B \int \mathrm{PST}(\theta)\sin(\theta)\mathrm{d}\theta. \tag{9}$$

3 Analysis Results of the Prototype

3.1 *Ghost Images*

In the prototype system, the doublets and the filter are coated with antireflection coating. Its reflectivity is 1.0% over the spectral range. The DOEs are composed of substrate and surface microstructure. The substrates are uncoated, so the reflectivity is 4.0%. The diffraction efficiency of microstructure is calculated according to Eq. (1). The ghost images results at the wavelength of 550 nm are shown in Figs. 3(a) and 3(b). The color scale shows the relative irradiance increasing from blue to red. In Fig. 3(a), the map of intensity distribution is in the linear space. Only the ghost image from the -first-order diffraction is obvious, that is to say it is the most serious ghost image. In Fig. 3(b), the map of intensity distribution is in the logarithmic space, where several ghost images appear. The ghost images are not focused at the image plane, but the focal point of these ghost images are near the image plane, so we also be careful to deal with that ghost images. From the results, we can find that the ghost images of the prototype come from two kinds of paths. One is the reflection of filter and the other is the same order diffraction of the DOE1 and the DOE2.

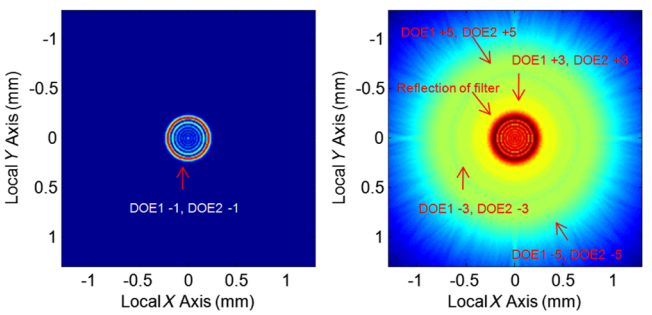

Fig. 3 On-axis ghost irradiance plots. Only ghost images are shown. Left is linear scale and right is Log scale.

3.2 *PST Calculation Result*

The RMS roughness of optical surfaces is tested by white light interferometer; the results are shown in Table 3. The surface TIS is calculated by Eq. (5) and the b_0 is determined by the method described in Sec. 2.2.

Figure 4 shows the PST curves in log space from 0.5 deg to 80 deg. When the off-axis angle is less than 25 deg, the sample interval is 0.5 deg and 5 deg for off-axis angle greater than 25 deg. There are some interesting features in the plots. The source outside the field of view can directly reach the detector by the nondesign order diffraction of DOE1. For angles less than 22.5 deg, the diffraction of DOE1 contributes the most stray light flux. Beyond 22.5 deg, the light scatter from DOE1 is dominant. Figure 4 shows the PST in different sections and the main contribution path. In the calculation, we only consider the diffraction from −7 to +9, because the efficiency of higher orders is less than 0.5%.

3.3 *Estimate of the VGI*

The flux reaching the detector is determined by

$$\Phi = \int_{\lambda_1}^{\lambda_2} S(\lambda)\tau(\lambda)V(\lambda)\mathrm{d}\lambda, \tag{10}$$

Table 3 RMS roughness and TIS of the optical surface.

Surface	Doublet and filter	Front of DOE	Back of DOE
RMS roughness (nm)	0.991	1.550	5.014
TIS, $\lambda = 0.55$ (%)	0.0034% (K9 glass) 0.0054% (ZF1 glass)	0.0066	0.0687
b_0	0.17 for K9 glass and 0.27 for ZF1 glass	0.033	3.46

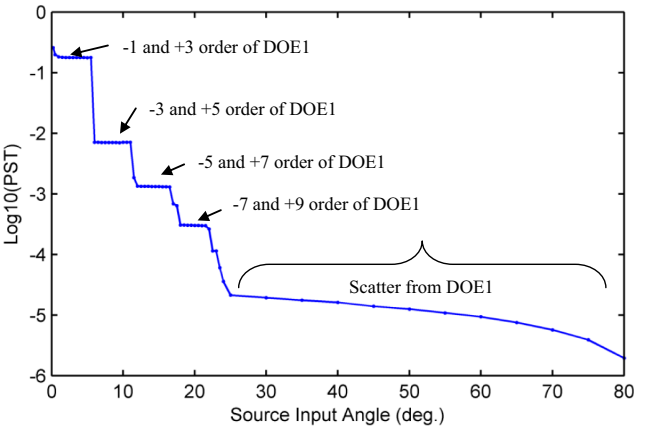

Fig. 4 The PST of the prototype system.

where $S(\lambda)$ is the spectral power, $\tau(\lambda)$ is the spectral transmittance of the system, and $V(\lambda)$ is the spectral response function of the detector which is equal to the visibility function. To take these effects into account, the flux was calculated at 17 wavelengths from 490 to 650 nm with equal intervals. The total flux equals the sum of these results and the irradiance is the flux divided by the area of the detector. Using Eqs. (7)–(9), the calculated VGI is 57.88%. When counting the stray flux according to the paths, the direct incident stray flux caused by nondesign diffraction of DOE1 accounts for 93.97% of the total stray flux. So, the best way to reduce the VGI of diffractive telescope is improving the diffraction efficiency of the diffractive primary lens.

4 Test Results of the Prototype

4.1 *Ghost Images*

In Sec. 3.1, the ghost irradiance was analyzed at the wavelength of 550 nm. But in application, the light source is polychromatic. At different wavelength, the diffraction efficiency and the light deflection ability of DOEs will change according to Eqs. (1) and (2). So the distribution of the ghost irradiance will change correspondingly. Considering that factor, the spectral range was divided into 17 small segments. The ghost irradiance was analyzed at the middle wavelength of each segment. The 17 results were superposed and shown in Fig. 5(a). The center of the plot has been truncated to show the detail of ghost irradiance around the image point. To obtain the ghost distribution, the exposure time of charge-coupled device was improved when getting the star image of the prototype. When the intensity of star image is saturation, the ghost images appear around the image as shown in Fig. 5(b). The test results are in accordance with the simulation results; while the actual size of the ghost distribution is 0.58 mm, larger than the calculated value 0.53 mm. This difference may be caused by the fabrication error and assembly error of the prototype.

4.2 *VGI of the Prototype*

According to the ISO9358:1994,[19] a VGI test platform was built as shown in Fig. 6. The integral sphere with diameter of 1.5 m is used to simulate the background. The luminance uniformity is better than 3%. The detector is low light level illumination meter and the indication error is less than 4%.

The calculated value and the test result of VGI are shown in Table 4. The calculation value is 57.88% and the test result is 67.11%. The agreement in magnitude shows the correctness of the analytical methods. The difference between calculated value and test value may be caused by two factors. First, only the diffractive order between −7 and +9 was considered. The total diffractive efficiency is about 95%, the other orders will obviously increase the stray flux. Second, the processing errors of the DOE were not taken into account. These errors will reduce the efficiency of the +1 order and increase the efficiency of some nondesign orders.

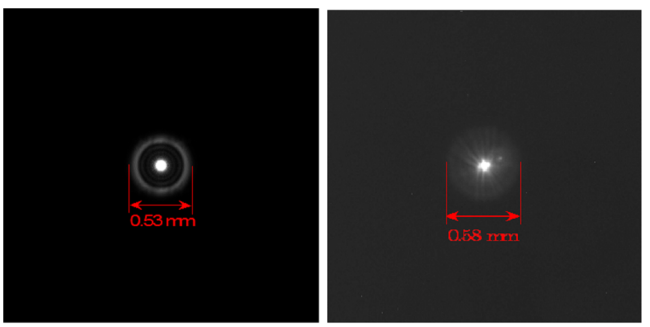

Fig. 5 The ghost irradiance around the star image of the prototype system. Left is the calculated results and the right is the test results.

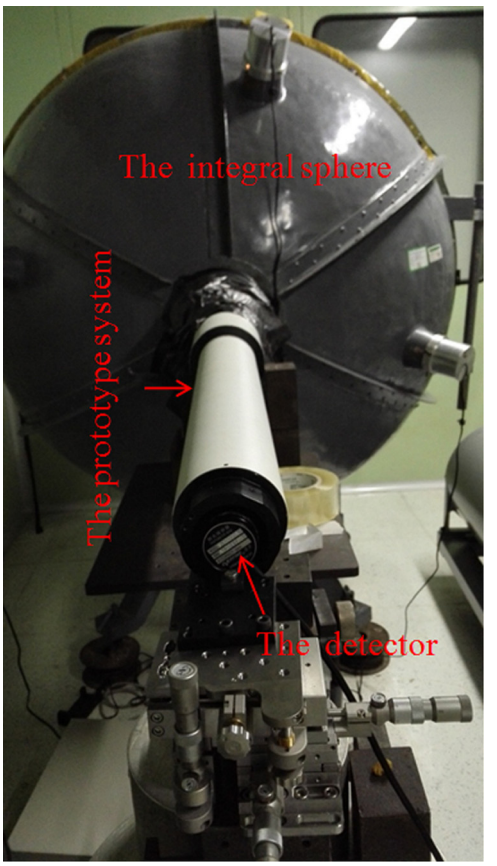

Fig. 6 VGI test of the prototype system.

Table 4 The VGI of the prototype.

	Test result	Calculated value
VGI	67.11%	57.88%

5 Summary and Conclusions

In this paper, the stray light characteristics of the diffractive telescope were analyzed comprehensively. For the diffractive telescope system, except for the residual reflections of the optical elements, the nondesign order of DOEs is an important cause of the ghost. The ghost path is mainly the same order diffraction of the diffractive primary lens and the achromatic DOE. The source outside the field of the view can directly illuminate the image plane through the nondesign order of diffractive primary lens according to the analysis of the PST. This stray light path contributes to more than 90% of the stray light flux on the image plane. Therefore,

improving the diffraction efficiency of the diffractive primary lens is the key to suppression of stray light in diffractive telescopes. In the future, further studies on effective measures to suppress stray light and improve imaging performance will be in progress.

Acknowledgments

This work was supported by the National Key R&D Program of the Ministry of Science and Technology of the People's Republic of China, grant No. 2016YF0500200 and the Chinese Academy of Sciences, grant No. YA16K010.

References

1. S. Roose et al., "The challenges for large light-weight diffractive lenses for space telescopes," *Proc. SPIE* **10563**, 105635Y (2014).
2. W. Yang et al., "Research advances and key technologies of macrostructure membrane telescope," *Opto-Electron. Eng.* **44**(5), 475–482 (2017).
3. H. A. MacEwen and J. B. Breckinridge, "Large diffractive/refractive apertures for space and airborne telescopes," *Proc. SPIE* **8739**, 873904 (2013).
4. L. Xiaotong et al., "Paraxial analysis of stray light caused by multi-order diffraction and multi-reflection," *Proc. SPIE* **5627**, 20–24 (2005).
5. D. A. Buralli and G. M. Morris, "Effects of diffraction efficiency on the modulation transfer function of diffractive lenses," *Appl. Opt.* **31**(22), 4389–4396 (1992).
6. H. Zhang et al., "Modified phase function model for kinoform lenses," *Appl. Opt.* **47**(22), 4055–4060 (2008).
7. T. Ando et al., "Diffraction light analysis method for a diffraction grating imaging lens," *Appl. Opt.* **53**(11), 2532–2538 (2014).
8. L. Koechlin et al., "Generation 2 tested of Fresnel imager: first results on the sky," *Exp. Astron.* **30**, 165–182 (2011).
9. L. Koechlin et al., "New progress on the Fresnel imager for UV space astronomy," *Astrophys. Space Sci.* **354**, 147–153 (2014).
10. P. Atecheson et al., "MOIRE-ground demonstration of a large aperture diffractive transmissive telescope," *Proc. SPIE* **9143**, 91431W (2014).
11. J. A. Britten et al., "Large-aperture fast multilevel Fresnel zone lenses in glass and ultrathin polymer films for visible and near-infrared imaging applications," *Appl. Opt.* **53**(11), 2312–2316 (2014).
12. R. Wang et al., "Effects of fabrication errors on diffractive efficiency for a diffractive membrane," *Chin. Opt. Lett.* **14**(12), 120501–120506 (2016).
13. G. Swanson, "Binary optics technology: theoretical limits on the diffraction efficiency of multilevel diffractive optical elements," Technical Report, Massachusetts Institute of Technology (1991).
14. J. E. Harvey, "Light scattering characteristics of optical surfaces," *Proc. SPIE* **0107**, 41–47 (1977).
15. J. Bennett and L. Mattsson, *Introduction to Surface Roughness and Scattering*, 2nd ed., pp. 66–67, Optical Society of America, Washington, DC (1999).
16. E. C. Fest, *Stray Light Analysis and Control*, pp. 140–141, SPIE Press, Bellingham, Washington (2013).
17. Institute of Environmental Sciences and Technology, "Product cleanliness levels and contamination control program," IEST-STD-CC1246D, Institute of Environmental Sciences and Technology (2002).
18. P. Spyak and W. Wolfe, "Scatter from particulate-contaminated mirrors. Part 2: theory and experiment for dust and $\lambda = 0.6328$ μm," *Opt. Eng.* **31**(8), 1757–1763 (1992).
19. ISO, "Optics and optical instruments—veiling glare of image forming systems—definitions and methods of measurement," 1994, ISO 9358:1994, https://www.iso.org/standard/17042.html (2014).

Dun Liu was a PhD student at the University of Chinese Academy of Sciences (UCAS). In 2013, he received his bachelor's degree at Wuhan University. He has been conducting the research of diffractive telescope technology at the Institute of Optics and Electronics (IOE), Chinese Academy of Sciences, from 2013 to present. His current research interests include optical design and stray light analysis and testing.

Lihua Wang has been an associate researcher at IOE since 2017. Her research topics include optical design and subaperture stitching testing of large aperture optical systems.

Wei Yang has been an associate researcher at IOE since 2010. Her research topics include membrane optical imaging technology, integrated simulation, and automatic testing technology of optical systems.

Shibin Wu has been a research director since 2006 at IOE. His research topics include optical testing and precision instruments. He is a member of the Chinese National Optical Metrology Committee.

Bin Fan has been a research director since 2013. His research topics include advanced manufacturing technology of large aperture aspheric surface and advanced optical testing. He is a member of SPIE.

Fan Wu is a senior research at IOE and a PhD tutor at UCAS. His research topics include advanced optical manufacturing and testing technology. He is the secretary general of the Optical Manufacturing Committee of the Chinese Optical Society.